Hindawi Publishing Corporation
International Journal of Optics
Volume 2012, Article ID 962317, 6 pages
doi:10.1155/2012/962317

Research Article

Optimization of *s*-Polarization Sensitivity in Apertureless Near-Field Optical Microscopy

Yuika Saito, Yoshiro Ohashi, and Prabhat Verma

Department of Applied Physics, Osaka University, 2-1 Yamadaoka, Suita, Osaka 565-0871, Japan

Correspondence should be addressed to Yuika Saito, yuika@ap.eng.osaka-u.ac.jp

Received 31 August 2011; Revised 27 October 2011; Accepted 14 November 2011

Academic Editor: Alexandre Bouhelier

It is a general belief in apertureless near-field microscopy that the so-called *p*-polarization configuration, where the incident light is polarized parallel to the axis of the probe, is advantageous to its counterpart, the *s*-polarization configuration, where the incident light is polarized perpendicular to the probe axis. While this is true for most samples under common near-field experimental conditions, there are samples which respond better to the *s*-polarization configuration due to their orientations. Indeed, there have been several reports that have discussed such samples. This leads us to an important requirement that the near-field experimental setup should be equipped with proper sensitivity for measurements with *s*-polarization configuration. This requires not only creation of effective s-polarized illumination at the near-field probe, but also proper enhancement of s-polarized light by the probe. In this paper, we have examined the *s*-polarization enhancement sensitivity of near-field probes by measuring and evaluating the near-field Rayleigh scattering images constructed by a variety of probes. We found that the *s*-polarization enhancement sensitivity strongly depends on the sharpness of the apex of near-field probes. We have discussed the efficient value of probe sharpness by considering a balance between the enhancement and the spatial resolution, both of which are essential requirements of apertureless near-field microscopy.

1. Introduction

Apertureless near-field scanning optical microscopy (ANSOM) is becoming more and more popular for its application to a variety of nanoscale samples, where one can do microscopic as well as spectroscopic analysis at nanoscale [1, 2]. The key feature of ANSOM is enormous enhancement and confinement of light field at the apex of the near-field probe, which is a sharp metallic nanotip. The enhancement of scattered light from a sample can be more effective under proper polarization. Thus near-field imaging through ANSOM combined with proper control of polarization provides even more information about the sample, such as molecule and crystal symmetry, orientation, intermolecular interaction, optical transition, and so forth. In fact, many researchers have occasionally employed polarization-controlled ANSOM to enhance the contrast of measurements [3–7]. Under a reflection-type (or side-illumination-type) near-field setup where the incident and scattered lights are in opposite directions, the optical configuration makes it easy to conveniently control the polarization of incident light at the tip apex. For this reason, the method of polarization control has been widely used for the analysis of nanoscale anisotropy, such as the crystalline structure, for reflection-type systems [8–13]. On the other hand, in a more commonly used transmission-type ANSOM configuration, where the incident and scattered lights are in the same direction, it is not easy to control the polarization, and hence one can find very few experimental reports on the polarization measurement in this type of experimental setup [14–16]. Even when a polarization control is employed in ANSOM setup, it is mostly to study the *p*-polarization configuration. One reason is that the *p*-polarization of excitation can form a strongly enhanced light source under the sharp apex of the near-field probe [17, 18], which also gives strong enhancement to the scattering from the sample in most of the cases. However, if one is studying the optical mode of a sample that has a dipole transition perpendicular to the probe axis, the *p*-polarization is no longer suitable. In this case, one needs to arrange the

s-polarization enhancement by the near-field probe. Indeed several experimental reports suggested that ANSOM probes show *s*-polarization sensitivity [19, 20], though none of them discussed it clearly.

In this study, we will provide an experimental evidence of the *s*-polarization sensitivity in apertureless near-field probes. Our near-field probes are fabricated by coating a thin layer of metal on a sharp dielectric nanotip. The sharpness of the tip apex depends on the thickness of the metallic layer. We prepared near-field probes with varying metal thickness and employed them to measure near-field Rayleigh scattering images under *s*-polarized illumination by scanning the tip over the focused laser spot. The method has been employed to evaluate the surface plasmon behavior [21], and such scattering images also are indicators of the polarization sensitivity of the enhancement by the near-field probes. We have discussed the *s*-polarization sensitivity of various probes through the contrast in the corresponding scattering images. In addition, we have also performed some calculations and computer simulations to obtain supportive information for checking the tendency polarization sensitivity on the sharpness of the near-field probe. We make a note that even though the simulation indicates that less sharpened probes with larger apex tend to give better enhancement for the *s*-polarized light, they are not ideal probes for near-field imaging because they lose the spatial confinement of the light. Thus one can find an optimum value of probe sharpness by evaluating the system sensitivity and the requirement of spatial resolution.

2. Experimental

The apertureless near-field probes were prepared by coating thin layers of silver on commercially available atomic force microscopy (AFM) cantilevers made of silicon (CSG01 tips purchased from NT-MDT co.). Silver coating was performed by the method of vacuum evaporation under a high vacuum of 2×10^{-6} Torr. By controlling the evaporation parameters, the probes were prepared with silver coating of 20, 40, and 60 nm. Since it was difficult to prepare thicker layers of silver under the same condition, we utilized simultaneous annealing at 400°C during the evaporation, to achieve the silver layer thickness of about 150 nm. The apex sharpness for all the silver-coated probes was checked by scanning electron microscope (SEM).

The optical setup for our near-field measurement is illustrated in Figure 1, which shows a system based on inverted microscope [22, 23]. The incident laser (CW, $\lambda = 488$ nm) is expanded 20 times in diameter and is introduced via various optical components to the inverted microscope. In order to achieve an *s*-polarized incident light at the near-field probe, we first prepared azimuthal polarization of the propagating laser by using a spatially patterned $\lambda/2$ waveplate (*z*-pol from Nanophoton). This waveplate can realizes a perfect *x*-*y*-polarization as shown in the inset in Figure 1. The detailed explanation of how the waveplate works was shown in [23]. The experiment was done by utilizing a high-NA objective lens ($\times 60$, NA = 1.4, oil emersion) to focus the light on the probe and by inserting an optical mask on the beam path that rejects the low-NA component (NA < 1) of the incident light. The near-field probe was set on an AFM stage and was scanned over the tightly focused laser spot. Rayleigh scattered signal was collected by the same objective lens in low-NA (NA < 1) configuration, which was detected by a photodiode. In the case of *s*-polarization excitation the scattering signal from the tip apex is efficiently collected in the low NA region because of the emission pattern of the dipole [24]. Moreover, the incident light that was introduced in an evanescent illumination configuration can be effectively reduced by the detection aperture, which results in the reduction of background signal in detection. The probe was scanned at the steps 30 nm to cover a scanning area of about 1 μm in square.

The simulation for a 2D finite difference time domain (FDTD) calculation was performed by using R-soft with nonuniform mesh. Since this is a rough estimation just to check the trend, we have employed 2D simulation instead of 3D. The quantitative difference between 2D and 3D is not an issue in this estimation. The probe apex was assumed to be a single silver sphere with different diameters, which was placed 2 nm above a glass substrate (index 1.5). The *s*-polarized incident light was launched at an angle of 45° from the substrate to achieve an evanescent illumination under the condition of total internal reflection. The field intensity was monitored 10 μm downward from the particle to anticipate the far field intensity.

3. FDTD Simulations

In order to understand the effect of polarization on the near-field enhancement in the proximity of a probe, we first made a rough estimation through FDTD simulation. Although a silver nanoparticle considered in simulation can never represent the real near-field probe prepared by silver evaporation, it still gives correct information about the trend that a real probe would follow on enhancement. For simplicity, we considered an ellipsoid-shaped nanoparticle with an aspect ration of 1 : 4. Figure 2 shows the enhancement in the proximity of the nanoparticle for both *p*- and *s*-polarizations, which was calculated following the method of Moon and Spencer [17]. The horizontal dashed line represents the sample plane. As one can see, the light field is greatly enhanced near the apex (between the nanoparticle and the sample plane) for *p*-polarized illumination, whereas it is significantly enhanced at the middle area of the nanoparticle for the *s*-polarized illumination. As one goes away from the middle area towards the apex, the enhancement decreases and becomes very weak near the apex area. This result confirms that the enhancement near the sample is very weak for *s*-polarization, and hence *p*-polarization is a preferred configuration for most near-field experiments. However, if we consider scattering in the far field (when the detector is placed far from the probe apex), there are rooms for the *s*-polarization to be scattered back within the cone angle of the objective lens. To see if this happens, we performed numerical simulations by keeping the detector far from the

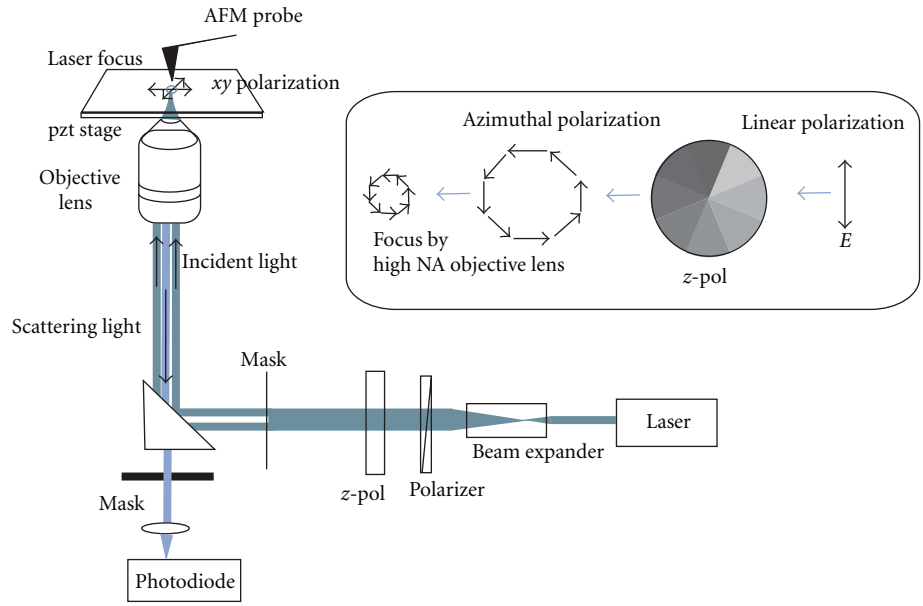

Figure 1: Experimental setup of near-field probe scanning over the laser focus in *s*-polarization condition. The inset illustrates a schematic of *s*-polarization formation by using *z*-pol.

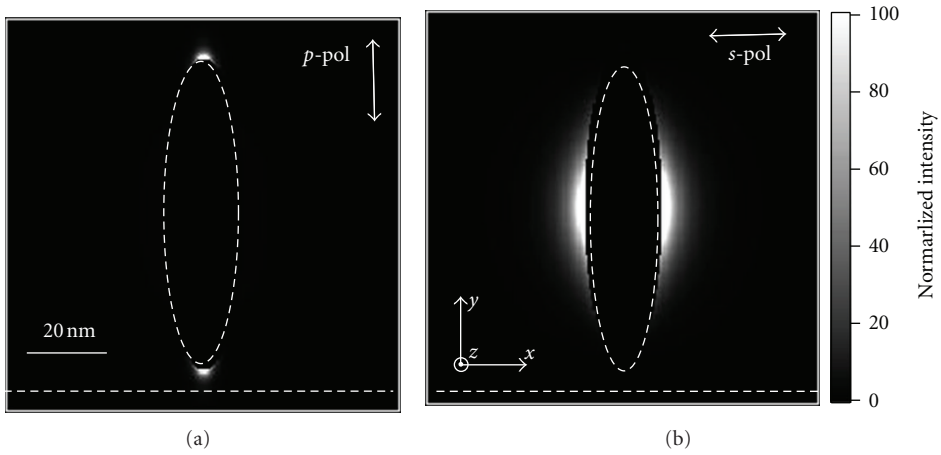

Figure 2: Theoretical calculation of electric field distributions near an ellipsoidal metallic nanoparticle under (a) *p*-polarization and (b) *s*-polarization excitations. The horizontal dotted lines indicate the sample surface. Strong field confinement can be seen near the apex between the sample and the probe in *p*-polarization, which is almost negligible in *s*-polarization.

probe. We also considered the effect of sharpness of the probe apex on the far-field enhancement, for which we approximated the probe apex by a single spherical silver particle and varied the diameter of that particle. Figure 3 shows some FDTD simulation results for far-field scattering under evanescent illumination employing *s*-polarization excitations for varying apex size. The simulation conditions are illustrated in the inset. As one can see in Figure 3, the far-field enhancement under *s*-polarized illumination has a significant dependence on the apex size. The scattering intensity shows relatively small rise for the apex diameter varying from 0 to ~20 nm, then it monotonically increases with the apex diameter. This brings us to a conclusion that the scattering efficiency for *s*-polarization illumination increase, as the particle size increases, or as the apex sharpness decreases. The signal intensity becomes almost double for a probe with the diameter of 50 nm as compared to 30 nm. This is a reasonable figure for the net enhancement that is in accordance with our experimental statistics.

4. Results and Discussions

We anticipate from the calculation that the *s*-polarization sensitivity of a near-field probe increases as the sharpness of the probe apex decreases. As discussed before, the near-field probes used in this study were prepared by coating a thin silver layer on silicon nanotips. The apex of the silicon tip

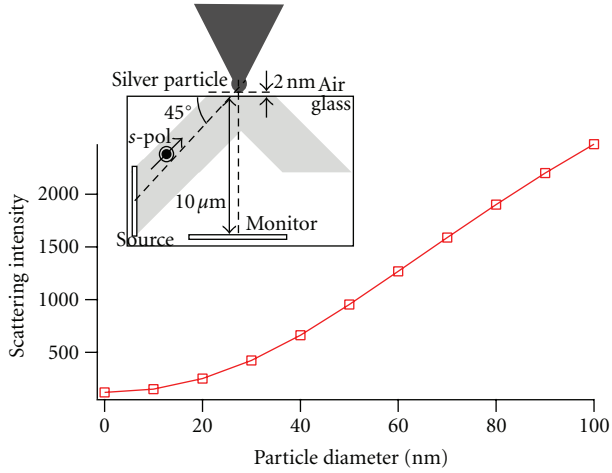

Figure 3: FDTD simulation of *s*-polarization scattering intensity from silver particle with respect to the apex diameter. Inset illustrates the simulation conditions.

is quite sharp; however the sharpness of the probe decreases as the thickness of the silver layer coated on the silicon tip increases. Even though the entire shape of the real probe is different from the probes used in FDTD simulation, we expect a similar trend of enhancement as the thickness of the silver layer on the probe increases. That means we expect the *s*-polarization sensitivity of the probes with thicker silver layers to be higher than that for the probes with thinner silver layers. Figures 4(a)–4(d) show SEM images of probes that have silver layers with thickness 0, 20, 40, and 60 nm, respectively. A closer look at the probe apex in these SEM images reviles that the apex diameter of the probe increase gradually as the coating thickness increases. Figures 5(a)–5(d) show Rayleigh scattering images of *s*-polarized laser spot measured by employing the probes shown in Figures 4(a)–4(d), respectively. Doughnut-shaped patterns could be seen in these Rayleigh scattering images, which is an evidence of *s*-polarization condition. The contrast variation in these images corresponds to the scattering efficiency for excitation light. Since we created *s*-polarized illumination at the probe apex by introducing the high-NA component of an azimuthally polarized laser beam, a comparison of image contrast in Figure 5 can be considered as the comparison of *s*-polarization sensitivity of the probes [25]. We also calculated the quantitative values of contrast by a simple relation

$$\text{contrast} = \frac{\left(I_S - I_{Bg}\right)}{\left(I_S + I_{Bg}\right)}, \quad (1)$$

where I_S indicates the signal intensity corresponding to the signal area (laser spot) and I_{Bg} denotes the background intensity corresponding to the background area. The net intensities were the summations over the measured areas. Table 1 shows the contrast values obtained from (1) for different probes. As seen in Figure 5(a), we could not get any image pattern under *s*-polarization for the noncoated probe in Figure 4(a), because this bare silicon probe did not have an *s*-polarization sensitivity. The contrast is still

Table 1: Contrast of the probes shown in Figure 5, as calculated from (1).

Tip	Diameter/nm	Contrast
a	5	0
b	20	0.023
c	40	0.037
d	60	0.061

weak in Figure 5(b) for the probe with silver thickness of 20 nm; however, it becomes stronger in Figure 5(c) when the silver layer on the probe is as thick as 60 nm. This result is consistent with the simulation results in Figure 3, where the tip apex is approximated as a single silver particle. It is not appropriate to make a quantitative comparison however, it is clear that the scattering intensity monotonously increases as the particle size increases.

One may expect from the simulation results that a broader probe would scatter more light under *s*-polarization, thus further increasing the probe size may result in an enormous enhancement. However, experimentally this was not true. The Rayleigh scattering image contrast decreased for the broader probe ~150 nm in apex diameter. This may come from the surface plasmon resonance wavelength of the coated silver, which is shifted to longer wavelength for larger structure; however the reason is still unclear. Apart from this decrease in scattering efficiency, a probe with larger apex diameter also degrades the spatial resolution in the measurement. Thus a probe with larger apex diameter is not suitable for near-field studies. This leads us to the conclusion that the *s*-polarization efficiency of a near-field probe can be increased by increasing the apex diameter of the probe, however, up to a certain limit where the spatial resolution is still acceptable.

The optimum value of probe apex diameter that can give best results for both *s*-polarization sensitivity and spatial resolution in near-field measurement would depend on the experimental system and requirement. In general, a near-field probe that can provide contrast of about 0.03 is acceptable for a good-quality imaging. In our case, the probes shown in Figures 4(c) and 4(d) provide acceptable contrast, and hence they qualify for *s*-polarization ANSOM experiments. We can thus conclude that a 30–60 nm-thick silver coating can result in reasonably good near-field probe for enhancement of *s*-polarization. The lower limit can still be changed by optimizing the collection efficiency of the optical setup, and the upper limit can be determined by the requirement of spatial resolution. For tips with more efficient *s*-polarization sensitivity, the on-gap mode tips could provide good results [26]. However, fabrication of a gap as small as ~1 nm at the tip apex is difficult with current technology, and hence it is still not in practical use. Therefore, the best way to achieve the *s*-polarization sensitivity at this moment is to carefully control the size of the probe apex by optimizing evaporation parameters.

Finally, we would also like to make a small note on the *p*-polarization sensitivity of these probes. Instead of the azimuthal polarization, using radial polarization of incidence

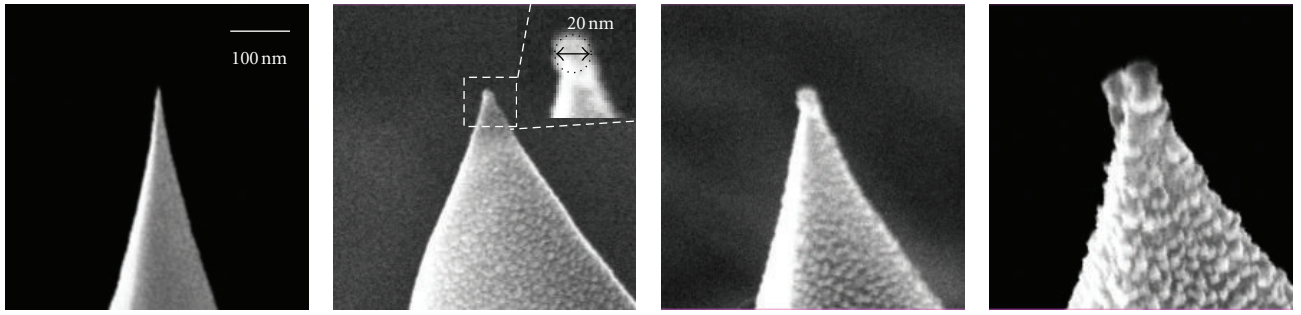

Figure 4: SEM images of several ANSOM probes with varying thickness of silver coating. (a) Bare silicon probe with no silver coating, (b) probe with 20 nm silver coating, (c) probe with 40 nm silver coating, and (d) probe with 60 nm silver coating. The zoomed inset shows how we estimate the apex size.

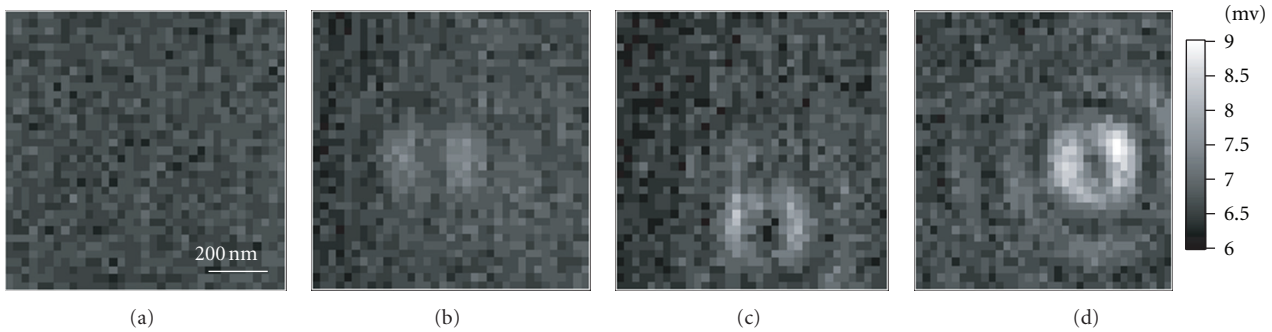

Figure 5: Scattering images of the *s*-polarization laser focus measured by the probes with different silver coatings. The images (a)–(d) correspond to the probes shown in Figures 4(a)–4(d), respectively. The contrasts in the images correspond to the *s*-polarization sensitivities of these probes.

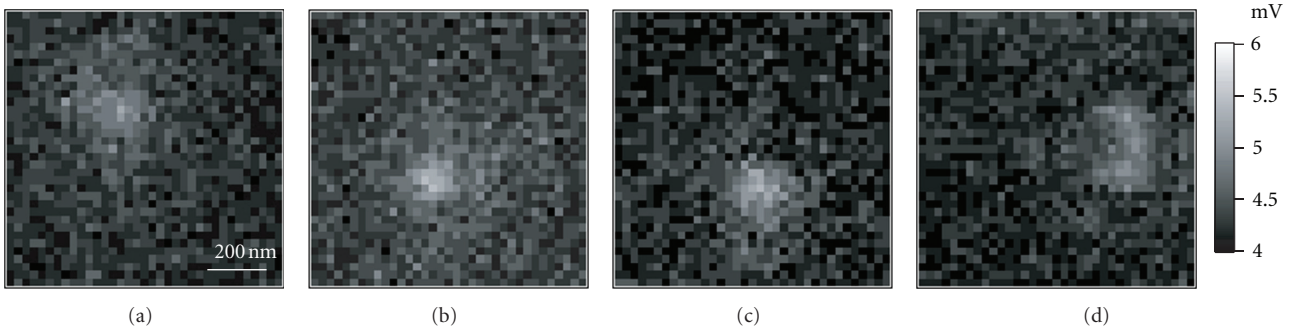

Figure 6: Scattering images of the *p*-polarization laser focus measured by the probes with different silver coatings. The images (a)–(d) correspond to the probes shown in Figures 4(a)–4(d), respectively.

laser beam can result in the dominant generation of *p*-polarization at probe apex. By utilizing radial polarization, we measured the Rayleigh scattering images for the same probes that were discussed earlier in Figure 4. The results are shown in Figures 6(a)–6(d), which corresponds to the *p*-polarization sensitivity. Since the *p*-polarization dipole was not efficiently collected in this experimental configuration, the image did not show a strong contrast. Nevertheless, every probe shows certain amount of *p*-polarization sensitivity even if they did not have *s*-polarization sensitivity such as the uncoated probe shown in Figure 4(a).

5. Conclusions

In conclusion, we have examined the enhancement phenomena of ANSOM probes for their *s*-polarization sensitivities, which could be extremely important for those samples,

which have optical response in the direction perpendicular to the probe axis. A supporting FDTD simulation as well as experimental results showed that the probes with larger apex diameter yield stronger scattering when illuminated with *s*-polarized light. However, the experimental results also indicated that the contrast could not be improved only by increasing the diameter of the apex. We conclude that the metal coating thicker than 30 nm is necessary for *s*-polarization sensitivity in our system. For further improvement of *s*-polarization sensitivity in ANSOM measurements, there could still be some scope for optimizing the probe design, including the possibility of estimations through calculations and simulations [27, 28].

References

[1] Y. Saito and P. Verma, "Imaging and spectroscopy through plasmonic nano-probe," *EPJ Applied Physics*, vol. 46, no. 2, Article ID 20101, 2009.

[2] P. Verma, T. Ichimura, T. A. Yano, Y. Saito, and S. Kawata, "Nano-imaging through tip-enhanced Raman spectroscopy: stepping beyond the classical limits," *Laser and Photonics Reviews*, vol. 4, no. 4, pp. 548–561, 2010.

[3] N. Lee, R. D. Hartschuh, D. Mehtani et al., "High contrast scanning nano-Raman spectroscopy of silicon," *Journal of Raman Spectroscopy*, vol. 38, no. 6, pp. 789–796, 2007.

[4] M. Motohashi, N. Hayazawa, A. Tarun, and S. Kawata, "Depolarization effect in reflection-mode tip-enhanced Raman scattering for Raman active crystals," *Journal of Applied Physics*, vol. 103, no. 3, Article ID 034309, 2008.

[5] P. G. Gucciardi, M. Lopes, R. Déturche, C. Julien, D. Barchiesi, and M. Lamy De La Chapelle, "Light depolarization induced by metallic tips in apertureless near-field optical microscopy and tip-enhanced Raman spectroscopy," *Nanotechnology*, vol. 19, no. 21, article 215702, 2008.

[6] A. Merlen, J. C. Valmalette, P. G. Gucciardi, M. Lamy de la Chapelle, A. Frigout, and R. Ossikovski, "Depolarization effects in tip-enhanced raman spectroscopy," *Journal of Raman Spectroscopy*, vol. 40, no. 10, pp. 1361–1370, 2009.

[7] M. P. Nikiforov, S. C. Kehr, T. H. Park et al., "Probing polarization and dielectric function of molecules with higher order harmonics in scattering-near-field scanning optical microscopy," *Journal of Applied Physics*, vol. 106, no. 11, Article ID 114307, 2009.

[8] D. A. Higgins, D. A. Vanden Bout, J. Kerimo, and P. F. Barbara, "Polarization-modulation near-field scanning optical microscopy of mesostructured materials," *Journal of Physical Chemistry*, vol. 100, no. 32, pp. 13794–13803, 1996.

[9] S. C. Schneider, S. Grafström, and L. M. Eng, "Scattering near-field optical microscopy of optically anisotropic systems," *Physical Review B*, vol. 71, no. 11, Article ID 115418, pp. 1–8, 2005.

[10] G. Picardi, Q. Nguyen, R. Ossikovski, and J. Schreiber, "Polarization properties of oblique incidence scanning tunneling microscopy-tip-enhanced raman spectroscopy," *Applied Spectroscopy*, vol. 61, no. 12, pp. 1301–1305, 2007.

[11] Z. H. Kim and S. R. Leone, "Polarization-selective mapping of near-field intensity and phase around gold nanoparticles using apertureless near-field microscopy," *Optics Express*, vol. 16, no. 3, pp. 1733–1741, 2008.

[12] S. Berweger and M. B. Raschke, "Polar phonon mode selection rules in tip-enhanced Raman scattering," *Journal of Raman Spectroscopy*, vol. 40, no. 10, pp. 1413–1419, 2009.

[13] M. Chaigneau, G. Picardi, and R. Ossikovski, "Molecular arrangement in self-assembled azobenzene-containing thiol monolayers at the individual domain level studied through polarized near-field raman spectroscopy," *International Journal of Molecular Sciences*, vol. 12, no. 2, pp. 1245–1258, 2011.

[14] E. J. Sánchez, L. Novotny, and X. S. Xie, "Near-field fluorescence microscopy based on two-photon excitation with metal tips," *Physical Review Letters*, vol. 82, no. 20, pp. 4014–4017, 1999.

[15] Y. Saito, N. Hayazawa, H. Kataura et al., "Polarization measurements in tip-enhanced Raman spectroscopy applied to single-walled carbon nanotubes," *Chemical Physics Letters*, vol. 410, no. 1–3, pp. 136–141, 2005.

[16] W. Chen and Q. Zhan, "Numerical study of an apertureless near field scanning optical microscope probe under radial polarization illumination," *Optics Express*, vol. 15, no. 7, pp. 4106–4111, 2007.

[17] P. Moon and D. E. Spencer, *Field Theory for Engineers*, Van Nost. Reinhold, 1961.

[18] S. Kawata, Y. Inouye, and T. Sugiura, "Near-field Scanning Optical Microscope with a laser trapped probe," *Japanese Journal of Applied Physics*, vol. 33, no. 12a, pp. L1725–L1727, 1994.

[19] A. Hartschuh, E. J. Sánchez, X. S. Xie, and L. Novotny, "High-resolution near-field Raman microscopy of single-walled carbon nanotubes," *Physical Review Letters*, vol. 90, no. 9, article 095503, pp. 1–4, 2003.

[20] T. A. Yano, P. Verma, Y. Saito, T. Ichimura, and S. Kawata, "Pressure-assisted tip-enhanced Raman imaging at a resolution of a few nanometres," *Nature Photonics*, vol. 3, no. 8, pp. 473–477, 2009.

[21] A. Bouhelier, F. Ignatovich, A. Bruyant et al., "Surface plasmon interference excited by tightly focused laser beams," *Optics Letters*, vol. 32, no. 17, pp. 2535–2537, 2007.

[22] N. Hayazawa, Y. Saito, and S. Kawata, "Detection and characterization of longitudinal field for tip-enhanced Raman spectroscopy," *Applied Physics Letters*, vol. 85, no. 25, pp. 6239–6241, 2004.

[23] Y. Saito, P. Verma, K. Masui, Y. Inouye, and S. Kawata, "Nano-scale analysis of graphene layers by tip-enhanced near-field Raman spectroscopy," *Journal of Raman Spectroscopy*, vol. 40, no. 10, pp. 1434–1440, 2009.

[24] Y. Saito, M. Kobayashi, D. Hiraga et al., "Z-polarization sensitive detection in micro-Raman spectroscopy by radially polarized incident light," *Journal of Raman Spectroscopy*, vol. 39, no. 11, pp. 1643–1648, 2008.

[25] Y. Saito, M. Honda, Y. Moriguchi, and P. Verma, "Temporally dynamic photopolymerization of C60 molecules encapsulated in single-walled carbon nanotubes," *Physical Review B*, vol. 81, no. 24, Article ID 245416, 2010.

[26] J. N. Farahani, H. J. Eisler, D. W. Pohl et al., "Bow-tie optical antenna probes for single-emitter scanning near-field optical microscopy," *Nanotechnology*, vol. 18, no. 12, Article ID 125506, 2007.

[27] R. Ossikovski, Q. Nguyen, and G. Picardi, "Simple model for the polarization effects in tip-enhanced Raman spectroscopy," *Physical Review B*, vol. 75, no. 4, Article ID 045412, 2007.

[28] P. Biagioni, J. S. Huang, L. Duò, M. Finazzi, and B. Hecht, "Cross resonant optical antenna," *Physical Review Letters*, vol. 102, no. 25, Article ID 256801, 2009.